Reducing Transmission Loss of the High Temperature Superconducting Power Cable

Kazuo Watanabe,[1] *Hikaru* Hidaka,[2] *Kazuya* Akashi,[2] *Yasuhiro* Iijima,[2]
Kunihiro Naoe,[2] *Ryo* Kikutake,[3] *Masakatsu* Nagata,[3] *Huminori* Tateno,[3]
Masanori Daibo,[3] and *Manabu* Yoshida[4]

High temperature superconducting (HTS) cables are expected to be adapted to compact type large power transmission cables. HTS cables have not only high current density and low AC loss but also some environmental merits such as energy saving, CO_2 gas reduction and magnetic shielding. In general, HTS tapes of the HTS conductor and shield layer in the HTS cables are wound in a spiral manner, and become a multi-layer winding with large current. As a result, since the HTS conductor and shield layer has a multiple coil structure with different winding pitches, the internal magnetic flux is generated in the longitudinal direction. Therefore, the eddy current loss is generated in the former of such HTS AC cables. In addition, since the eddy current is induced in circumferential direction in the cryostat pipe in the case of the single-core cable, the joule loss is generated. It is considered that the magnitude of the magnetic flux (loss) depends on the winding direction, winding pitch of the HTS tape and the magnitude of the current, and comes actualized together with the large current. Therefore, in order to reduce the loss of the entire cable, each loss reduction for the former, the HTS conductor, the HTS shield and the cryostat pipe is necessary. In this paper, these low-loss measures of Fujikura Ltd are reported. Together, analytical considerations utilizing elliptic functions are also introduced.

1. Introduction

Superconductivity is a phenomenon that certain materials exhibit exactly zero electrical resistance when cooled below a characteristic temperature. Since the discovery of the superconductivity phenomenon in 1911 by the Dutch physicist Heike Kamerlingh Onnes, various superconducting materials have been discovered. In 1986 and thereafter, oxide superconductors, which exhibit superconductivity when cooled with liquid nitrogen (77 K = −196 °C), have been found. Because the temperature at which superconductivity appears (critical temperature) of these oxide superconductors is dramatically high as compared to the case of the superconductors discovered in the earlier times, the oxide superconductors are called high temperature superconductors, and the superconductors discovered in the earlier times are called low temperature superconductors or metal superconductors. Among the high temperature superconductors, yttrium-based superconductors show high performance even in a magnetic field, and are expected to find a wide range of applications as high-temperature superconducting wires. Fujikura successfully developed its own method of ion-beam-assisted-deposition (IBAD) in 1991 [1)], and since then, has strenuously continued the development of yttrium-based superconducting wires.

Fujikura has also been positively developing coils for applications in magnet technology as applications for devices, in parallel with the development of the high performance wire [2)]. Furthermore, its application to large current and low loss superconducting cables, which is one example application in which the high critical current (Ic) wire is the most effective, is highly desirable, and the yttrium-based wire (IBAD-PLD wire), which has a critical current of the world's largest class amplitude of 500 A/cm-w (at 77 K, s.f.) or more, was applied to a 66 kV-5 kA_{rms} power cable for the first time in the last fiscal year (FY2012) of a commissioned project, "Technological Development of Yttrium-Based Superconducting Power Equipment" from the New Energy and Industrial Technology Development Organization (NEDO). Superconducting cables have advantages in energy savings, CO_2 emission reduction, and magnetic shielding for external magnetic field cancellation, in addition to having the features of high current density and low AC loss, and therefore superconducting cables are expected to find application as compact power cables for large capacity (large current) power transmission. Unlike DC cables in which no power loss arises in principle because of zero electrical resistance, in the case of AC cables, AC

1 Chiba University
2 Energy Technology Research Department of Advanced Technology Laboratory
3 New Business Development Center
4 Power EPC Systems Division

losses arise due to magnetic hysteresis inside the superconductor or other factors. The reason why the yttrium-based wire has been applied to the 66 kV-5 kA_{rms} power cable is that the yttrium-based wire is high in critical current density per unit cross-section area and is likely to give low AC losses, and the expected low AC losses were verified [3].

The greatest electrical features of superconducting cables are the characteristics of low voltage, large current (large capacity) and low loss. In the future, there is concern that AC loss at each structural part of the cable may become non-negligible when the current is increased, in addition to the loss at the superconducting conductor and the shield; in other words, concern that the AC loss includes eddy current loss that arises at each structure part due to the internal axial magnetic field, which is caused by the multi-coil structure of the conductor and the shield specific to large current superconducting cables. It is indispensable to reduce the AC loss at each structure part of cable in order to reduce the overall loss of the cable.

In this paper, Fujikura's measures for reducing losses in each structural part of the cable are reported. In addition, the paper presents how the complete elliptic integral of the first kind and the second kind as well as conformal mapping are utilized in analytical consideration.

2. Structure of superconducting power cable

The basic structure of a superconducting power cable is shown in Fig. 1. There are two types of structure for three-phase AC cables: triple-core type and single-core type. In the case of single-core type, three cables are required for three phases. For both types of cable, the superconducting conductor is constructed by spirally winding multiple layers of superconducting tape wire around a copper former. The structure and appearance of Fujikura's yttrium-based superconducting wire is shown in Fig. 2 as an example of a superconducting wire. The copper former, constructed by stranded copper wire, provides mechanical stiffness and serves as a branch to divert a large current in case of an accident from the superconducting conductor. An electrical insulation is a composite insulation consisting of insulating paper impregnated with liquid nitrogen. Externally to the electrical insulation, a super-

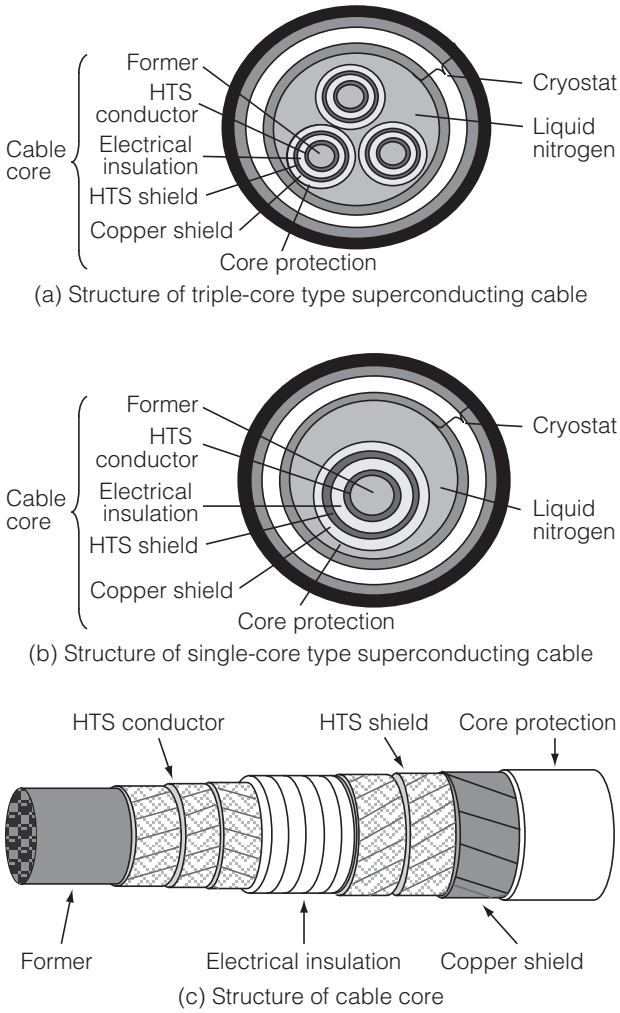

Fig. 1. Structure of superconducting power cable.

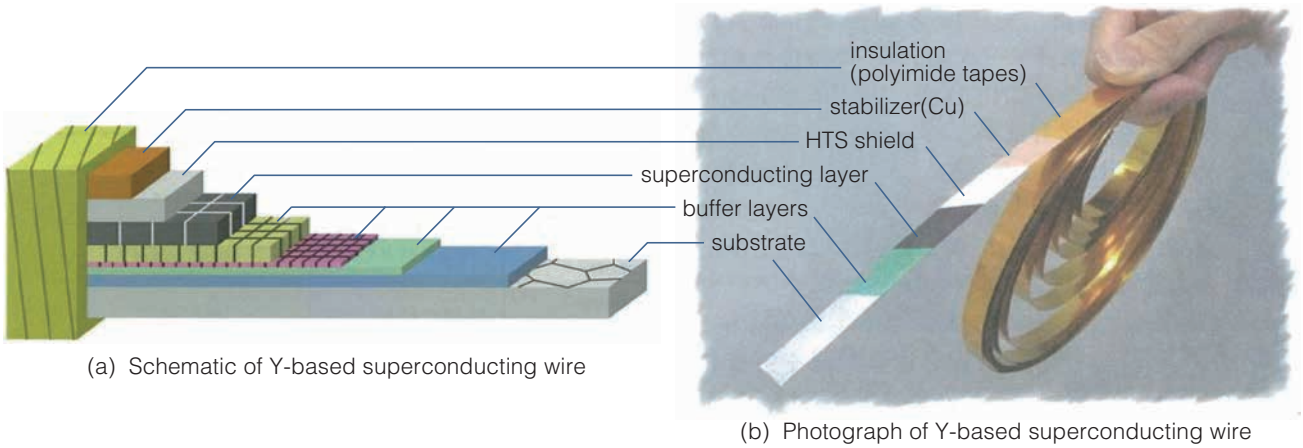

Fig. 2. Schematic of the structure and photograph of yttrium(Y)-based superconducting wires.

conducting shield layer consisting of multiple layers of spirally-wound superconducting wire is formed; in the superconducting shield layer, electric currents of nearly the same magnitude as the conductor current in the opposite direction are induced, shielding external magnetic fields due to the conductor current. Externally to the superconducting shield layer, a copper shield layer consisting of copper tape or copper string is wound, serving as a branch to divert a large current in case of an accident. A protection layer is wound in the outermost layer, completing a cable core. In the case of triple-core type, a cryostat is provided externally to the stranded three cores. The gap between the cores and the cryostat serves as a flow path of cooling liquid nitrogen. The cryostat is a vacuum-thermal insulation corrugated double pipe made of stainless steel. An anticorrosive layer is provided on the outside of the cryostat.

3. Internal axial magnetic field of superconducting cable

Let us consider the external circumferential magnetic field and the internal axial magnetic field of the cable core shown in Fig. 1(c). When the superconducting wires of both the conductor layer and the shield layer are straight longitudinally lapped (infinite strand pitch), the induced current in the shield is of the same magnitude as the conductor current in the opposite direction, and the circumferential magnetic field external to the shield layer is zero, as is the internal axial magnetic field. In the case of spiral winding, however, it is not possible to make both magnetic fields zero simultaneously. This will be shown in the following. For simplicity, assume the following as shown in Fig. 3 : the conductor layer consists of a single layer, the shield layer consists of a single layer, and the direction of strand is the same for both the conductor and the shield. The current is induced in the shield so that the total of the number of the magnetic flux interlinkage due to the conductor current and the shield current is reduced to zero. The number of the flux interlinkage is the sum of the number of external circumferential magnetic flux and the number of internal axial magnetic flux. The first term and the second term in Eq. (1) represent the number of the axial flux

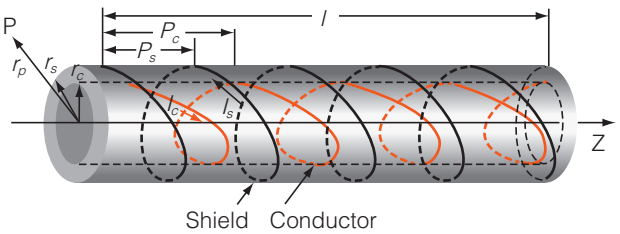

Fig. 3. An example of structure of a conductor layer and a shield layer.

interlinkage and the external circumferential flux interlinkage due to the conductor current, respectively, and similarly, the third term and the fourth term represent the number of the corresponding magnetic flux due to the shield current, respectively.

$$\mu_0 \frac{l}{P_s}\frac{I_c}{P_c}\pi r_c^2 + \frac{\mu_0 I_c l}{2\pi}\ln\frac{r_p}{r_s} - \mu_0 \frac{l}{P_s}\frac{I_s}{P_s}\pi r_s^2 - \frac{\mu_0 I_s l}{2\pi}\ln\frac{r_p}{r_s} = 0 \quad \cdots\cdots(1)$$

$$\therefore I_c\left(\frac{\pi r_c^2}{P_s P_c} + \frac{1}{2\pi}\ln\frac{r_p}{r_s}\right) = I_s\left(\frac{\pi r_s^2}{P_s^2} + \frac{1}{2\pi}\ln\frac{r_p}{r_s}\right) \cdots(2)$$

where,

P_c : Conductor strand pitch P_s: Shield strand pitch

r_c : Conductor radius r_s: Shield radius

r_p : Distance from the conductor center to an arbitrary point, P

I_c : Conductor current I_s: Current induced in the shield

l : Cable length under consideration

The term r_p, may be assumed to be the phase spacing in the case of a reciprocating single-phase current circuit of parallel configuration and of a balanced three-phase current circuit of triangular configuration.

When the following condition is satisfied in Eq.(2), $I_c = I_s = I$ is obtained, whereby the magnetic field external to the shield layer is reduced to zero.

$$\frac{r_c^2}{P_s P_c} = \frac{r_s^2}{P_s^2} \quad \cdots\cdots(3)$$

From Eq. (3),

$$P_s = \left(\frac{r_s}{r_c}\right)^2 P_c \quad \cdots\cdots(4)$$

$$r_s > r_c \quad \text{giving,} \quad P_s > P_c$$

Consequently, different values are obtained for the internal axial magnetic fields H_c and H_s due to the conductor current and the shield current, respectively, as follows:

$$H_c = \frac{I}{P_c} > H_s = \frac{I}{P_s} \quad \cdots\cdots(5)$$

That is, if the magnetic field external to the shield layer could be made zero, the internal axial magnetic field could not be made zero simultaneously. However, the number of the flux interlinkage of the shield layer is reduced to zero.

Note : According to Eq.(2), note that there can be a solution in which $I_s > I_c$, or the current induced in the shield is larger than the conductor current.

4. Loss at each structure part of superconducting cable and measures for reducing the loss

In general, superconducting power cables consist of a multilayered conductor and a multilayered shield,

which are spirally wound (stranded) with an increasing number of superconducting wires when the current is increased. The uniform current distribution design is adopted for the design of the strand pitch of each layer so that the flux interlinkage between adjacent layers (the total sum of the number of circumferential magnetic flux interlinkage and the number of axial magnetic flux interlinkage) is reduced to zero [4]. Accordingly, a multi-coiled structure is formed in which the strand pitch is different for each layer. For the cable of multi-coiled structure, it is regarded, as described in the preceding section, that the circumferential magnetic field external to the shield layer and the internal axial magnetic field cannot be made zero simultaneously. As a result, it is anticipated that, if the magnetic field external to the shield layer can be made completely zero, the internal axial magnetic field still exists, inducing electric currents in each structure part of cable, in turn giving rise to Joule loss, as shown in Fig. 4. For the copper stranded wire former and the stainless-steel cryostat pipe, circumferential eddy currents arise due to the internal axial flux interlinkage. Moreover, even in the case of the copper shield layer of copper tape lap winding, circumferential eddy currents arise similarly, giving rise to Joule loss. Furthermore, eddy current losses are proportional to the square of the flux interlinkage or the magnitude of magnetic field (electric current), and there is concern that losses at each structure part of cable, which have been neglected thus far, may become non-negligible when the current is increased.

The measures for reducing losses of superconducting cable when the current is increased are shown in Fig. 5. Moreover, the sites of loss generation for cables of triple-core type and single-core type are given in Table 1. In the case of cables of triple-core type, the axial magnetic fields in the cryostat pipe are cancelled

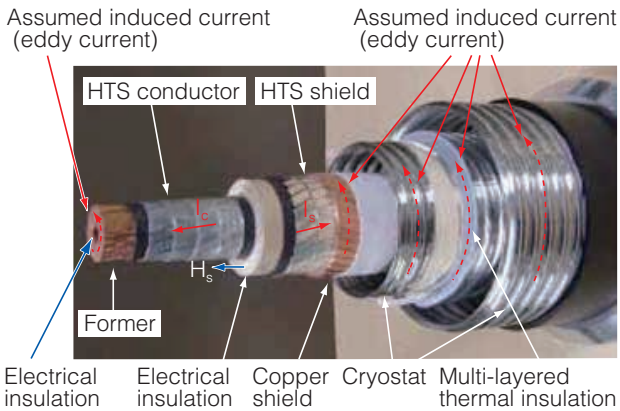

Fig. 4. AC loss generation part by internal longitudinal magnetic flux ofsingle-core HTS cable.

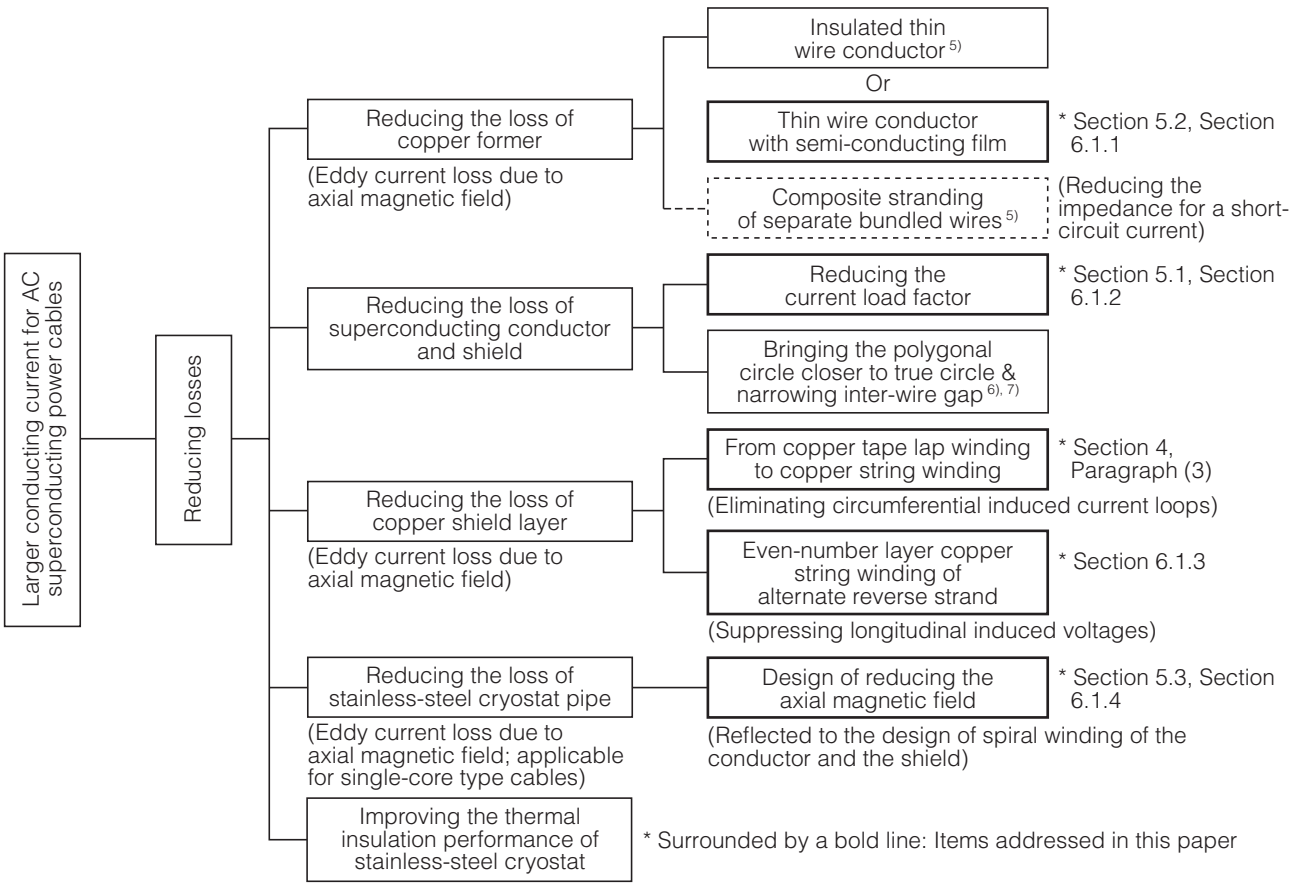

Fig. 5. The low-loss measures of HTS AC power cable with large current.

Table 1. AC loss generation site of the triple-core cable and single-core cable.

Site of generation of loss	Triple-core type	Single-core type
Copper former	○	○
Superconducting conductor and shield	○	○
Copper shield	○	○
SUS cryostat pipe	—	○

○ : Generation of loss

to zero due to balanced three-phase current, causing no eddy current loss in the cryostat. In the case of superconducting cables used for voltages of 66 kV or higher, the thickness of the electrical insulation increases, and at the same time, the size of the cable core increases because of the conductor and the shield consisting of an increased number of layers when the current is increased. For this reason, it is conceivable that the cable of single-core type may become a realistic choice associated with increase in voltage and current.

The measures surrounded by a bold line among Fujikura's measures for reducing losses given in Fig. 5 are described below.

(1) Reducing the loss of copper former

It is reported that insulated stranded wires are adopted as a measure for reducing the eddy current loss of copper stranded wire former, as mentioned earlier [5]. Our theoretical consideration showed that the adoption of a conductor with semi-conducting cupric oxide (CuO) film instead of a conductor made of insulated thin wire is equally effective for reducing the eddy current loss of copper former. Fujikura has developed the application of this semi-conducting film to normal conducting large size conductors with low loss, and the semi-conducting film has been successfully applied even for cryogenic cables. The application of the film has an advantage that connection work can be simplified for example.

(2) Reducing the losses of superconducting conductor and shield

Two different approaches for reducing losses of superconducting conductor and shield in the transmission of large AC currents are reported. One is to reduce losses by reducing the current load factor (I_t/I_c: the ratio of the amplitude I_t of AC transmission current to the critical current I_c); in this approach, it is necessary to greatly increase the critical current (I_c) of superconducting wire.

The other, which is reported by Amemiya et al.,[6) 7)] is to reduce the inter-wire gap, and at the same time, to change the cross-sectional arrangement of superconducting tape wires from a polygonal arrangement to a true circular arrangement. The actual conductor is formed by spirally-wound many tape wires of a certain

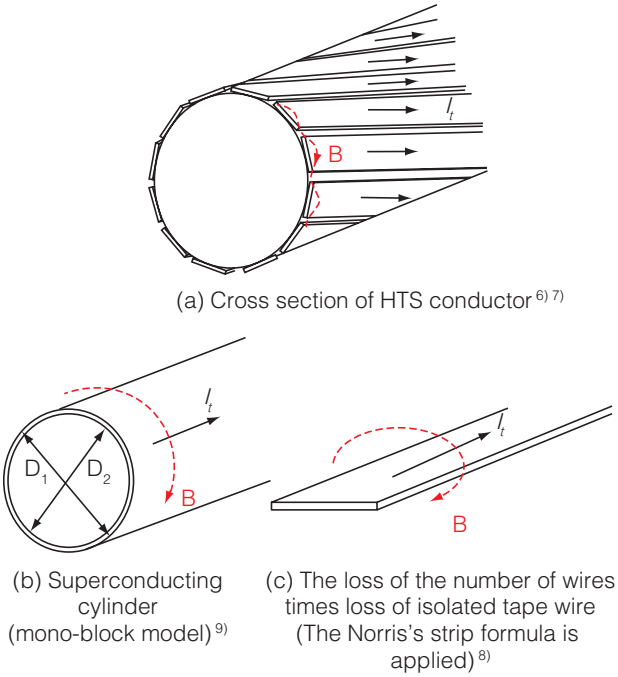

Fig. 6. Cross sections of HTS cable conductor, the superconducting cylinder model and an isolated superconducting strip model.

width, and therefore, the tape wires are arranged in a polygonal form in the cross section of conductor as shown in Fig. 6(a). The AC loss is said to be dominated by both the magnetic field component vertical to the face of tape wire, which arises due to the polygonal arrangement, and the vertical magnetic field component, which arises because of undulation of lines of magnetic force disturbed by inter-wire gap. It is argued that, from the viewpoint of reducing the magnetic field component vertical to the face of tape wire, an effective measure for reducing losses is to bring the cross section of conductor close to the true circle by reducing the tape width and increasing the number of wires, and at the same time, to suppress the circumferential undulation of the magnetic field by narrowing the inter-wire gap [6) 7)].

In this paper, the former approach of reducing the current load factor will be presented. In Section 6, demonstration tests on a trial specimen of low load factor cable made of high critical-current wire will be presented.

(3) Reducing the loss of copper shield

Since circumferential eddy currents arise in the cable of lap winding of copper tape, copper string winding is adopted in order to eliminate circumferential current loops. Conceivable means for the purpose include sparse winding, insulated tape winding of a single copper strip, and insertion of an insulation string. Then, however, the copper shield layer acts as a coil, inducing voltages in the longitudinal direction. Therefore, non-inductive winding is considered as a mea-

sure for reducing the induction.

(4) Reducing the loss of stainless-steel cryostat

Theoretical and experimental demonstration shows that the internal axial magnetic field is responsible for the eddy current loss in the cryostat. This loss is also taken into account in optimal design of the strand pitch for the conductor and the shield.

5. Reducing losses at each structure part of superconducting cable

5.1 Reducing the loss of superconducting conductor

Of the two approaches for reducing AC losses of superconducting conductor, the approach to reduce losses by reducing the current load factor I_t/I_c (I_t: the amplitude of AC transmission current) applicable for a large critical current I_c will be addressed in this paper.

For simplicity, we consider AC loss characteristics of a single-layer conductor. It is regarded that the AC loss of an actual conductor constructed by spirally-wound many wires as shown in Fig. 6(a) lies intermediate between the following two limiting cases:[6) 7)] one, the hysteresis loss (in the case of mono-block model[9)]) of a superconducting cylinder whose thickness is the same as that of the superconducting wire layer shown in Fig. 6(b), and the other, the loss of the number of wires times the hysteresis loss of a single tape wire shown in Fig. 6(c), which is calculated using the Norris strip formula[8)].

Firstly, we address the former, the case of the mono-block model. When a superconducting cylinder whose critical current is I_c transmits an AC current whose amplitude is I_t, the conduction loss per unit length of cylinder per one cycle of current change is given by the following equation[9)].

$$Q_{MB}=\frac{\mu_0 I_c^2}{2\pi h^2}\left\{\left(2-\frac{I_t}{I_c}h\right)\frac{I_t}{I_c}h+2\left(1-\frac{I_t}{I_c}h\right)\ln\left(1-\frac{I_t}{I_c}h\right)\right\} \quad \cdots(6)$$
$$h=\frac{D_1^2-D_2^2}{D_1^2}$$

where, D_1 and D_2 are the outside diameter and the inside diameter of the cylinder, respectively. In order to express Eq.(6) as a function of I_t and I_t/I_c, Eq.(6) is arranged to Eq.(7) by expanding the natural logarithm on the right side into an infinite series.

$$Q_{MB}=\frac{\mu_0 I_t^2}{\pi}\left(\frac{I_t}{I_c}h\right)\left\{\frac{1}{2\cdot3}+\frac{1}{3\cdot4}\left(\frac{I_t}{I_c}h\right)+\frac{1}{4\cdot5}\left(\frac{I_t}{I_c}h\right)^2+\frac{1}{5\cdot6}\left(\frac{I_t}{I_c}h\right)^3+\cdots+\frac{1}{(r+1)(r+2)}\left(\frac{I_t}{I_c}h\right)^{r-1}+\cdots\right\} \quad (7)$$

Secondly, we address the latter, the loss of the number of wires times the hysteresis loss of a single tape wire, which is calculated using the Norris's strip formula. The hysteresis loss per unit length due to self magnetic field of a single wire is given as follows:[8)]

$$Q_{t,N-s}=\frac{\mu_0 I_c^2}{\pi}\left\{\left(1-\frac{I_t}{I_c}\right)\ln\left(1-\frac{I_t}{I_c}\right)+\left(1+\frac{I_t}{I_c}\right)\ln\left(1-\frac{I_t}{I_c}\right)-\left(\frac{I_t}{I_c}\right)^2\right\} \quad \cdots\cdots(8)$$

Likewise, in order to express Eq.(8) as a function of I_t and I_t/I_c, Eq.(8) is arranged to Eq.(9) by expanding the natural logarithm on the right side into an infinite series. The number of wires times the result of Eq.(9) will give the AC loss of a superconducting conductor.

$$Q_{t,N-s}=\frac{\mu_0 I_t^2}{\pi}\left(\frac{I_t}{I_c}\right)^2\left\{\frac{1}{2\cdot3}+\frac{1}{3\cdot5}\left(\frac{I_t}{I_c}\right)^2+\frac{1}{4\cdot7}\left(\frac{I_t}{I_c}\right)^4+\frac{1}{5\cdot9}\left(\frac{I_t}{I_c}\right)^6+\cdots+\frac{1}{(r+1)(r+2)}\left(\frac{I_t}{I_c}\right)^{2(r-1)}+\cdots\right\} \quad \cdots(9)$$

Both Eq. (7) and (9) show that the current load factor I_t/I_c will be decreased and the loss will be reduced as the current I_c is improved while the transmission current I_t is kept constant. This behavior is depicted in Fig. 7. The normalized AC loss in the vertical axis represents the ratio to the loss when current load factor is 1. In the case of Fig. 7(a), Norris's strip model, the loss decreases significantly as the load factor is decreased from 1, and the slope (rate of decrease) becomes smaller at around the load factor of 0.5. On the other hand, in the case of Fig. 7(b), Mono-block model, the loss is very small compared to the Norris's strip model, because h in Eq.(6) is very small, on the order of 10^{-4}, because of the small thickness of several micrometers of the yttrium-based wire superconducting layer. The AC loss of actual conductors is considered to lie intermediate between the two limiting cases mentioned above, and is closer to the loss of the number of wires times the hysteresis loss of a single wire, which

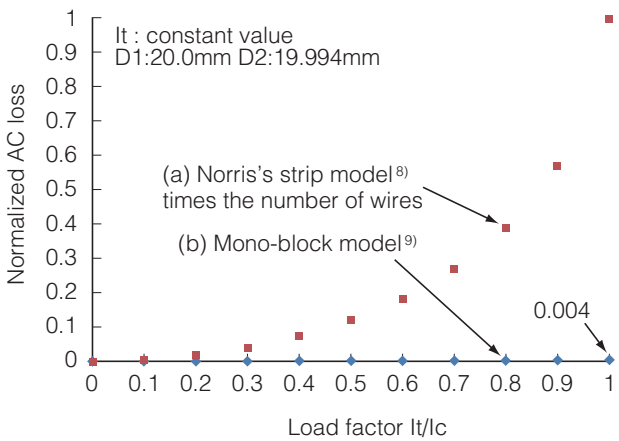

Fig. 7. Decrease in AC loss by the reduction of current load factor (It/Ic) under the transport current uniformity. (Norris's strip model and mono-block model)

is calculated using the Norris strip formula [6) 7)].

In this paper, as will be described in Section 6, the load factor is set to 50% at 77K for the transmission current of 5 kA_{rms} (amplitude $I_t = \sqrt{2} \times 5$ kA) by the use of a high critical current wire.

5.2 Reducing the loss of copper former [10)]

In this section, we will consider the relationship between the eddy current loss and the film resistivity when each wire of the copper former is a resistive film wire instead of an insulation film wire, and it will be shown that a loss reducing effect comparable to that for the insulation film can be expected for the semi-conducting film. Semi-conducting metal films include cupric oxide (CuO) film, which has been successfully applied to conductors for cryogenic cables [11)]. The film has an advantage that connection work can be simplified. Moreover, this film has been widely used also for large-size low-loss conductors for normal conduction [12)].

5.2.1 Eddy current losses of copper formers of cylindrical conductor and of insulated stranded wire

Firstly, we will calculate the eddy current loss of a basic solid cylindrical conductor. Consider the loss per unit length as illustrated in Fig. 8. The penetration depth, δ, into the conductor caused by the skin effect, of the magnetic flux in the conductor due to the axial magnetic field of the copper former is given by the following equation:

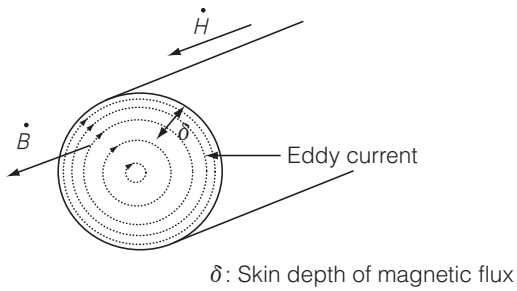

Fig. 8 Eddy current distribution for circular cylinder former.

$$\delta = \sqrt{\frac{2\rho_c}{\mu_0 \omega}} = 3.2[mm] \quad \cdots\cdots\cdots\cdots\cdots(10)$$

where,

$\mu_0 = 4\pi \times 10^{-7}[H/m]$

$\rho_c = 2 \times 10^{-9}[\Omega \cdot m]$ *at* 77K

$\omega = 2\pi f$

$f = 50[Hz]$

The eddy current flows circumferentially, and most of the eddy current flows through the outer layer with the skin depth δ of conductor due to the skin effect of magnetic flux. In the case of the copper former of insulated stranded wire, since the wire diameter is smaller than the penetration depth of magnetic flux, the eddy current flows circumferentially in entire cross-section of each of the stranded wires as shown in Fig. 10. Suppose that the circumferential eddy current through the shaded annular region in Fig. 9 is dominated by the resistance component of self impedance of the annular region; then, the resistance, dR, and the Joule loss, dW, are given as follows when the magnetic flux interlinked to the annular region is denoted as Φ:

$$dW = (d\Phi/dt)^2/dR \quad \cdots\cdots\cdots\cdots\cdots(11)$$

where, $\Phi = \mu_0 H \pi \left\{ r^2 - \left(\frac{D}{2} - \delta \right)^2 \right\}$ $\quad dR = \rho_c \frac{2\pi r}{dr}$

Then, the total eddy current loss is given by the following equation, if the magnetomotive force due to the eddy current is neglected:

$$W = \int dW = \frac{\pi(\omega\mu_0 H)^2}{2\rho_c} \int_{\frac{D}{2}-\delta}^{\frac{D}{2}} \frac{\left\{ r^2 - \left(\frac{D}{2} - \delta \right)^2 \right\}^2}{r} dr = \frac{\pi(\omega\mu_0 H)^2 G}{2\rho_c} \quad \cdots\cdots\cdots\cdots\cdots\cdots\cdots\cdots(12)$$

where, $G \frac{D^4}{64} - \left(\frac{D}{2} - \delta \right)^2 \frac{D^2}{4} + \left(\frac{D}{2} - \delta \right)^4 \left(\frac{3}{4} + \ln \frac{D}{D - 2\delta} \right)$

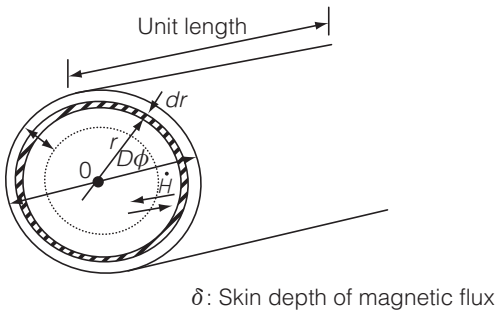

Fig. 9 Calculation model of eddy current loss for circular cylinder former.

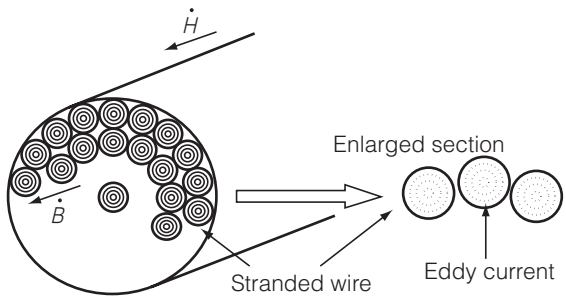

Fig. 10. Eddy current distribution for former with insulated wires.

Next, the eddy current loss per a stranded wire of the insulated stranded wire former can be obtained by the replacement of D with d (diameter of a stranded wire) and δ with $D/2$ in Eq. (12). The total eddy current loss, W_1, is given as follows by multiplying the number of stranded wires, n:

$$W_1 = \frac{n\pi(\omega\mu_0 H)^2}{8\rho_c}\frac{d^4}{16} \quad \cdots\cdots\cdots\cdots\cdots(13)$$

$n = \sum_{k=1}^{N} n_k$, n_k : Number of stranded wires in the kth layer

5.2.2 Eddy current loss of stranded wire former with resistive film

In this case also, the skin effect due to magnetic flux arises, and if the skin effect is neglected, estimated losses would be larger; however, this is on the safety side from the viewpoint of design, and the handling of analysis can be simplified. For this reason, the skin effect will be neglected hereafter in the consideration of eddy current loss. Because of stranded wire former with the resistive film (mainly semi-conducting film) instead of the insulated stranded wire former, we separately consider the eddy current in the single stranded wire in the center, and the eddy current through the circumferential stranded wires of each layer as shown in Fig. 11. Using Eq. (13) in the previous section, the eddy current loss, w_1, in the single stranded wire (assuming k = 1) in the center is given as follows:

$$w_1 = \frac{\pi(\omega\mu_0 H)^2}{8\rho_c}\frac{d^4}{16} \quad \cdots\cdots\cdots\cdots\cdots(14)$$

Now, we replace the volume resistivity, ρ_c, for the uniform current in the cylindrical conductor, with the equivalent volume resistivity, ρ_{ek}, by taking into account the increase in the resistance due to the restriction of circumferential current path of each layer because of limited contact area between adjacent stranded wires as well as due to the resistive film. Then, the eddy current loss of each layer (kth layer), w_k, is given by the following equation:

$$\begin{aligned} w_k &= \frac{\pi(\omega\mu_0 H)^2}{2\rho_{ek}}\int_{r_{k-1}}^{r_k} r^3\,dr \\ &= \frac{\pi(\omega\mu_0 H)^2}{8\rho_{ek}}(r_k^4 - r_{k-1}^4) \end{aligned} \quad \cdots\cdots\cdots\cdots(15)$$

where, r_k: outer radius of the kth layer, r_{k-1}: outer radius of the k-1th layer, k: 2nd to Nth layer

From Eq. (14) and (15), the total eddy current loss of the entire former, W_2, is given as follows:

$$\begin{aligned} W_2 &= w_1 + \sum_{k=2}^{N} w_k \\ &= \frac{\pi(\omega\mu_0 H)^2}{8}\left\{\frac{r_1^4}{\rho_c} + \sum_{k=2}^{N}\frac{r_k^4 - r_{k-1}^4}{\rho_{ek}}\right\} \end{aligned} \quad \cdots(16)$$

Here, suppose that the wire diameter is $d\phi$ for each layer; namely,

$$r_k - r_{k-1} = d \quad r_k = \frac{2k-1}{2}d \quad r_{k-1} = \frac{2k-3}{2}d$$

then,

$$W_2 = \frac{\pi(\omega\mu_0 H)^2}{8}\times\frac{d^4}{16}\left\{\frac{1}{\rho_c} + \sum_{k=2}^{N}\frac{(2k-1)^4 - (2k-3)^4}{\rho_{ek}}\right\} \cdots(17)$$

Next, we derive the equivalent volume resistivity of each layer, ρ_{ek}, which is the most important parameter in Eq. (16) and (17).

< Equivalent volume resistivity, ρ_{ek} >

In Fig. 12 and 13, we regard that the equivalent resistance of the resistive film stranded wire, R_e, is composed as follows:

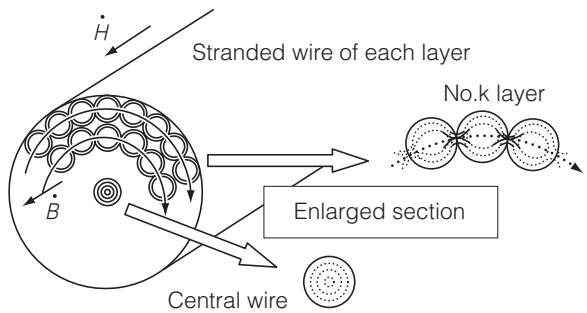

Fig. 11. Eddy current distribution for former with resistive film wires.

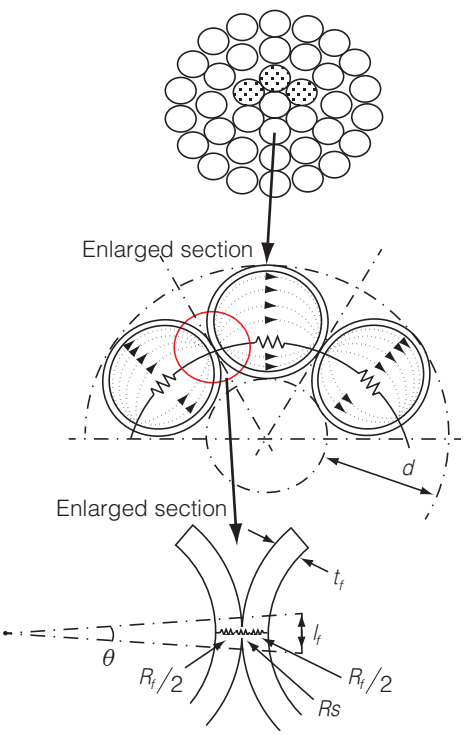

Fig. 12. Circumferential resistance of stranded wire former with resistive film.

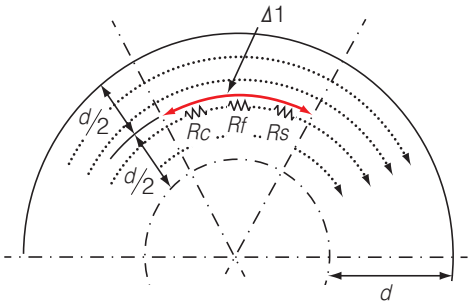

Fig. 13 Equivalent resistance for stranded wire former with resistive film

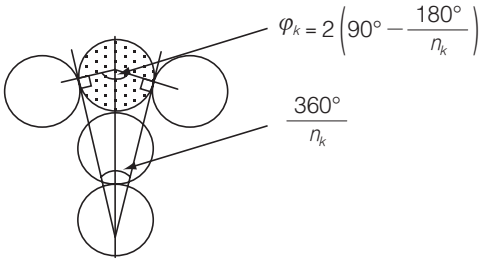

Fig. 14. Contact position of a strand wire with adjacent wires of both sides.

$$R_e = R_c + R_f + R_s = \rho_e \frac{\Delta l}{d \times 1} \cong \rho_e \frac{d}{d \times 1} = \rho_e \quad \cdots(18)$$

$$\because \Delta l \cong d \qquad R_f = \rho_f \frac{2t_f}{l_f \times 1}$$

where,

R_c: Concentrated resistance per unit length of the metal of stranded wire

R_f: Resistance per unit length of the resistive film at the contact area of stranded wires

R_s: Contact resistance per unit length of resistive films (not considered here)

ρ_c: Volume resistivity of the metal of stranded wire

ρ_f: Volume resistivity of resistive film

ρ_e: Equivalent volume resistivity of resistive film stranded wire

d: Diameter of a single stranded wire

t_f: Thickness of resistive film

l_f: Length of contact of stranded wires (circumferential direction) ($d/2 \times \theta\pi/180$)

θ: Center angle of the length of contact of stranded wires

φ_k: Contact angle of adjacent stranded wires (Fig. 14)

We will determine the relational expression between ρ_e (equivalent volume resistivity), ρ_c, and ρ_f: R_s is neglected here, because R_s cannot be decided uniformly, and the assumption of $R_s = 0$ will result in eddy current losses greater than true value, and will be on the safety side from the viewpoint of design. R_c (concentrated resistance of the metal of stranded wire) can be obtained by conformal mapping using an elliptic function (complete elliptic integral of the first kind) as described below. An accurate value of R_c can be derived theoretically using a model shown in Fig. 15(a). The relevant derivation process is presented in Fig. 15(a) through 15(e). The contact angle of adjacent stranded wires within the same layer (φ_k in Fig. 15(a)) depends on each layer. Now, regard the center wire as the layer of $k = 1$, and a graphical representation of φ_k for the kth layer is given in Fig. 14. The center angle of the length of contact of stranded wires is denoted as θ. The outline of the mapping process is described below. From Fig. 14 to Fig. 15(a): Enlarge the contact areas of the relevant stranded wire and the adjacent stranded wires, and regard the resultant arrangement as the original arrangement. From Fig. 15(a) to Fig. 15(b): Specify original coordinates of electrodes, which are normalized for calculation. From Fig. 15(b) to Fig. 15(c): Map the circular region into the complex upper half plane area using the following mapping function:

$$z = \frac{1-w}{1+w} i \qquad x = \tan\frac{\theta}{2} \quad \cdots\cdots\cdots\cdots(19)$$

From (c) to (d): Use the following linear function for the mapping from z-plane to Z-plane:

$$Z = \frac{\alpha z + \beta}{\gamma z + \delta} \quad \cdots\cdots\cdots\cdots\cdots\cdots(20)$$

where, α, β, γ, δ: Constants

Determine the respective coefficients for α, β, γ, and δ based on the correspondence between z-plane and Z-plane, and find the coordinate of point A, $1/k_1^2$. Denote the x coordinate of points A, P, Q, and R as a, p, q, and r, respectively.

$$k_1^2 = \frac{(r-q)(p-a)}{(a-q)(p-r)} = \frac{p(r-q)}{q(r-p)}$$
$$= \frac{\tan\frac{\theta}{2}\left\{\tan\frac{\varphi_k}{2} - \tan\frac{\varphi_k - \theta}{2}\right\}}{\tan\frac{\varphi_k}{2}\left\{\tan\frac{\theta}{2} + \tan\frac{\varphi_k - \theta}{2}\right\}} \quad \cdots\cdots\cdots(21)$$

From (d) to (e): Use the equation of a Legendre–Jacobi elliptic integral of the first kind (Eq. (22)) to map the upper half plane area of Z-plane into a rectangular region, and at the same time, arrange so that the electrodes are positioned on opposite sides. The length of these two sides is given by the complete elliptic integral (Eq. (23) and (24)). The modulus of an elliptic integral, k_1, is given by Eq. (21), and the complementary modulus, k_1', is determined by Eq. (25).

$$W = \int_0^Z \frac{dZ}{\sqrt{1-Z^2}\sqrt{1-k_1^2 Z^2}} \quad \cdots\cdots\cdots(22)$$

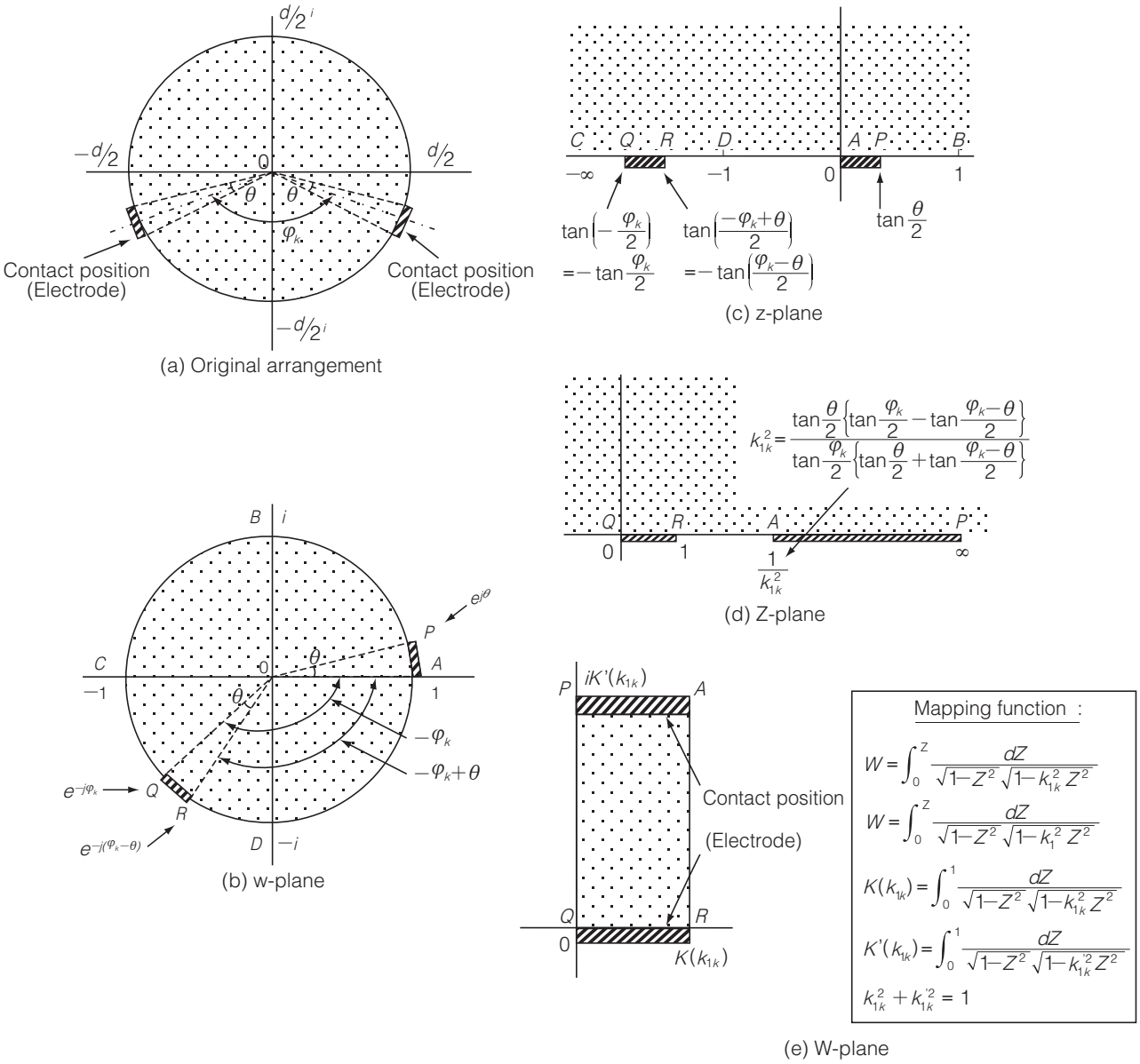

Fig. 15. Calculation process of concentrated resistance Rc of a strand wire.

$$K(k_1)=\int_0^1 \frac{dZ}{\sqrt{1-Z^2}\sqrt{1-k_1^2Z^2}} \quad \cdots\cdots(23)$$

$$K'(k_1)=\int_0^1 \frac{dZ}{\sqrt{1-Z^2}\sqrt{1-k_1'^2Z^2}} \quad \cdots\cdots(24)$$

$k_1^2+k'^2_1$ k_1: Modulus, k_1'
: Complementary modulus·····(25)

From the above, the concentrated resistance of the metal of stranded wire, R_c, is determined by the following equation:

$$R_c=\rho_c\frac{K'(k_1)}{K(k_1)} \quad \cdots\cdots(26)$$

Accordingly, from Eq. (18) and (26), the equivalent volume resistivity, ρ_e, is given by the following equation, which expresses the relationships among ρ_e, ρ_c, and ρ_f:

$$\rho_{ek}=\rho_c\frac{K'(k_{1k})}{K(k_{1k})}+\frac{2t_f}{l_f}\rho_f$$

$$k_{1k}^2=\frac{\tan\frac{\theta}{2}\left\{\tan\frac{\varphi_k}{2}-\tan\frac{\varphi_k-\theta}{2}\right\}}{\tan\frac{\varphi_k}{2}\left\{\tan\frac{\theta}{2}+\tan\frac{\varphi_k-\theta}{2}\right\}} \quad \cdots\cdots(27)$$

where, φ_k is the contact angle of adjacent stranded wires shown in Fig. 14.

$$\varphi_k=2\left(90^\circ-\frac{180^\circ}{n_k}\right)$$

$$l_f=\frac{d\theta\pi}{360}$$

From the above, the total eddy current loss of the entire former, W_2, is determined from Eq. (17) and (27).

5.2.3 Comparison of eddy current loss between resistive film wire former and insulated wire former

From the above, the "ratio of eddy current loss between the resistive film wire former and the insulated wire former," which is to be determined in the end, can be summarized from Eq. (13), (17), and (27) as follows:

$$\frac{W_2(\text{Resistive film wire})}{W_1(\text{Insulated wire})}=\frac{1}{n}\left\{1+\sum_{k=2}^{N}\frac{(2k-1)^4-(2k-3)^4}{\dfrac{K'(k_{1k})}{K(k_{1k})}+\dfrac{2t_f}{l_f}\cdot\dfrac{\rho_f}{\rho_c}}\right\}\quad\cdots\cdot(28)$$

where, $K(k_{1k})$ and $K'(k_{1k})$ are complete elliptic integrals of the first kind, and are determined from Eq. (23) and (24), respectively. k_{1k} and k_{1k}' are the modulus and complementary modulus, respectively, and are related as given in Eq. (25). k_{1k}^2 is given by Eq. (27). Equation (28) is meaningful only for $W_2 > W_1$.

On the other hand, the ratio, W_0/W_1, the ratio of eddy current loss between the non-coated stranded wire former (W_0) in the earlier times and the insulated film wire former (W_1), is given by the substitution of 0 for t_f or ρ_f in Eq. (28) as follows:

$$\frac{W_0(\text{Base wire})}{W_1(\text{Insulated wire})}=\frac{1}{n}\left\{1+\sum_{k=2}^{N}\frac{(2k-1)^4-(2k-3)^4}{\dfrac{K'(k_{1k})}{K(k_{1k})}}\right\}\quad\cdots\cdots\cdot(29)$$

Next, a trial calculation of W_2 (resistive film wire) / W_1 (insulated wire) using Eq. (28) is given below under the computational condition given below. Numerical calculation of a complete elliptic integral of the first kind can be readily performed at a high precision computation website on the Internet, and other computations can be made by hand calculation. The relationship between the eddy current loss and the film resistivity is plotted in Fig. 16.

< Computational condition >

Former outside diameter: D = 19 mm, Diameter of a single stranded wire: d = 2.8 mm, Total number of stranded wires: n = 37, n_1 = 1, n_2 = 6, n_3 = 12, n_4 = 18, Thickness of resistive film: t_f : 1 to 5 μm, Center angle of the length of contact: θ = 5º to 10º

In Fig. 16, the vertical axis represents the ratio to the eddy current loss of insulated wire former (W_1), and the horizontal axis represents the ratio of the resistivity of resistive film (ρ_f) to the resistivity of the metal of stranded wire (ρ_c). The graphs in Fig. 16(a) and 16(b) show that the ratio, W_2/W_1, is nearly 1 within the range where ρ_f/ρ_c, of higher than 10^4, suggesting that even the resistive film (including semi-conducting film) is equally effective in reducing the eddy current loss compared to the insulating film.

Note: Because the axial magnetic flux due to the eddy current above mentioned is small, an effect of canceling the original magnetic flux can be ignored.

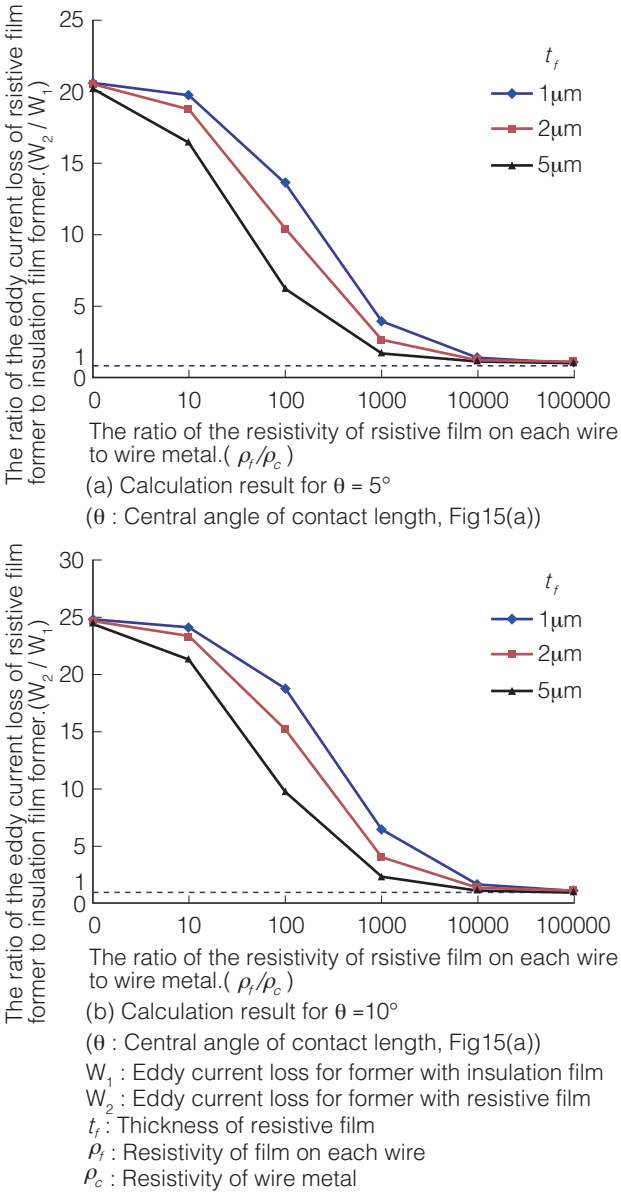

Fig. 16 Calculation result of eddy current loss vs. resistivity of resistive film.

5.3 Reducing the loss of cryostat pipe [13) 14) 15)]

As described above, the conductor and the shield of superconducting cables are constructed by spirally-wound numerous superconducting wires, constituting a multi-coil structure, and as a result, internal axial magnetic fields arise. In the case of single-core type AC superconducting cables, because of the internal axial magnetic field, axial flux interlinkage arises within the cryostat pipe, giving rise to eddy current loss. The magnitude of the magnetic flux (loss) depends on the standing direction, standing pitch, and the magnitude of current of each layer, and it is conceivable that it may become non-negligible when the current is increased. At this time, a formula for calculating the eddy current loss of cryostat pipe is derived. The formula is collated with actual measurement, and reflect-

ed in the design of a superconducting conductor and shield.

5.3.1 Formula for calculating the eddy current loss of cryostat pipe

The cryostat pipe is generally made of an stainless-steel corrugated double pipe, and the longitudinal cross section of a corrugated pipe with thickness of t is shown in Figure 17. Consider a very thin ring with the width of dx in this figure. The cross section of the thin ring is a parallelogram with a base of $t' = b + c$ and a height of dx. A loop current is induced within the very small ring, generating Joule loss.

The cross section, S, is $t'dx = (b + c)dx$.

$$b = a\tan\alpha \qquad c = a/\tan\alpha \qquad a = t\sin\alpha$$
$$\tan\alpha = y'(x) = dy/dx$$

$$\therefore t' = b + c = a(\tan\alpha + 1/\tan\alpha) = a(y' + 1/y') \cdots\cdots(30)$$

$$a = t\sin\alpha = t\frac{\tan\alpha}{\sqrt{1+\tan^2\alpha}} = t\frac{y'}{\sqrt{1+y'^2}} \cdots\cdots(31)$$

From Eq. (30) and (31).

$$t' = b + c = a(\tan\alpha + 1/\tan\alpha) = a(y' + 1/y')$$
$$= t\frac{y'}{\sqrt{1+y'^2}}\frac{1+y'^2}{y'} = t\sqrt{1+y'^2} \cdots\cdots(32)$$

Suppose that the corrugated pipe shown in Fig. 17 is an independent ring, and the shape of its outer surface is sinusoidal.

$$y = \frac{h}{2}\sin\frac{2\pi}{p}x + r_{mean} \qquad \therefore y' = \frac{h\pi}{p}\cos\frac{2\pi}{p}x \cdots\cdots(33)$$

The loop resistance of the thin ring is given as follows:

$$dR = \rho\frac{2\pi y}{t'dx} = \rho\frac{2\pi y}{t\sqrt{1+y'^2}dx} \cdots\cdots\cdots\cdots(34)$$

where, ρ: volume resistivity of stainless-steel cryostat pipe, t: thickness, r_{mean}: mean radius of corrugated pipe. In general, $t << r_{mean}$.

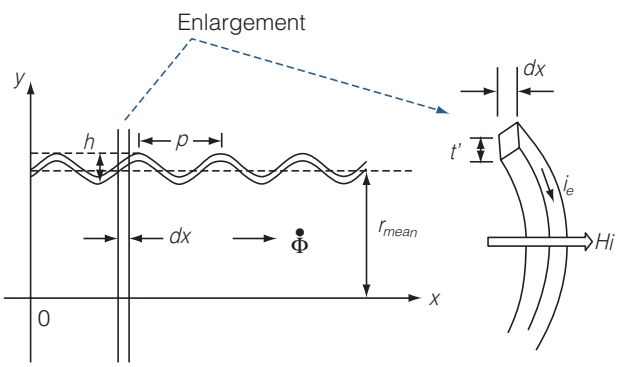

Fig. 17. Calculation using corrugated shape (Thin-ring).

When the material is stainless steel, the self impedance of the eddy current circuit of the thin ring is dominated by the resistance component, dR, (the reactance component can be neglected), and therefore, the eddy current loss, dW_{eddy}, is given as follows:

$$dW_{eddy} = \left|d\dot{\Phi}/dt\right|^2/dR = (\omega\Phi)^2/dR \cdots\cdots(35)$$

Substitution of dR with Eq. (34) and integration will give the eddy current loss per unit length of corrugated pipe, W_{eddy}.

$$W_{eddy} = \left|d\dot{\Phi}/dt\right|^2\int\frac{1}{dR} = (\omega\Phi)^2\int\frac{1}{dR}$$
$$= (\omega\Phi)^2\frac{t}{2\pi\rho}\int_0^1\frac{\sqrt{1+y'^2}}{y}dx$$
$$= (\omega\Phi)^2\frac{t}{2\pi\rho}\frac{1}{p}\int_0^p\frac{\sqrt{1+\left(\frac{h\pi}{p}\right)^2\cos^2\frac{2\pi}{p}x}}{\frac{h}{2}\sin\frac{2\pi}{p}x + r_{mean}}dx \cdots(36)$$

where, when the corrugation height is much smaller than the pipe size ($h << 2\,r_{mean}$), the denominator of the integrand is approximated by r_{mean}, and Eq. (36) is expressed as a complete elliptic integral of the second kind as shown in Eq. (37) and (38).

$$W_{eddy} = \frac{(\omega\Phi)^2 t}{2\pi r_{mean}\rho}\frac{1}{p}\int_0^p\sqrt{1+\left(\frac{h\pi}{p}\right)^2\cos^2\frac{2\pi}{p}x}\,dx$$
$$= \frac{2\pi\cdot f^2\cdot\Phi^2\cdot t}{\rho\cdot r_{mean}}\cdot K \cdots(37)$$

where, $\omega = 2\pi f$,

the shape factor, $K = \frac{2h}{p\cdot k}\cdot E\left(\frac{\pi}{2},\ k\right) \cdots\cdots\cdots\cdots(38)$

$E\left(\frac{\pi}{2},\ k\right)$: Complete elliptic integral of the second kind

$$\text{Modulus, } k = \left(\frac{h\pi}{p}\right)\Big/\sqrt{1+\left(\frac{h\pi}{p}\right)^2}$$

The shape factor, K, which depends on the pitch, p, and the corrugation height, h, of corrugation pipe, is determined as a function of a variable, h/p, and the table of shape factor is available [16]. Therefore, the eddy current loss due to internal axial flux interlinkage of the cryostat pipe of a single-core type AC superconducting cable can be easily computed by hand calculation from Eq. (37) and the table of shape factor given in Appended Table 1, when the dimensions, resistivity, and internal axial flux interlinkage of corrugation pipe are known.

Note: Because the axial magnetic field due to the eddy current above mentioned is small, an effect of canceling the original magnetic field can be ignored.

5.3.2 Eddy current loss of cryostat pipe: comparison with measured values

The eddy current loss of stainless-steel cryostat double pipe, whose dimensions are shown in Table 2, was measured by changing the internal axial magnetic flux interlinkage. The configuration of the loss-measuring circuit is illustrated in Fig. 19. A round-trip current is produced by means of short-circuiting the conductor and the shield at one end to eliminate the circumferential magnetic field external to the shield, and the conductor and the shield are stranded in opposite directions so that only the internal axial magnetic field remains. The eddy current loss of the cryostat pipe is obtained from the difference in the total loss of the conductor and the shield, with and without the cryostat pipe, by calculating losses $P = V \times I \times \cos\theta$, using the voltage, V, measured at the voltage-measuring leads attached to the conductor and the shield during the preparation of the measurement specimen, and the current, I, measured at the leads of current loading detection coil, and their phase difference, θ, which are fed into a lock-in amplifier. Both the inner pipe and outer pipe of the cryostat double pipe are immersed in liquid nitrogen during the measurement.

The measurement result is in good agreement with the calculated values as shown in Fig. 20. The calculated values obtained using the approximation formula (37), which are not shown in the figure, are also in agreement with the measurement result. This is because the dimensions of cryostat pipe shown in Table 2 satisfy the prerequisite for the approximation formula, $h << 2\,r_{mean}$.

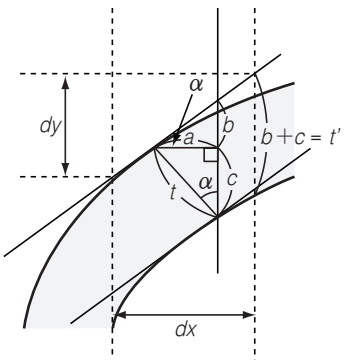

Fig. 18. Cross section of the thin ring for calculation.

Table 2. Dimensions of cryostat corrugated pipes.

Item	Inner pipe	Outer pipe
Inside diameter (mm)	64	100
Outside diameter (mm)	70	110
Average diameter $2r_{mean}$ (mm)	67	105
Corrugation height h (mm)	2.5	5
Thickness t (mm)	0.5	0.6
Corrugation pitch p (mm)	7.5	9

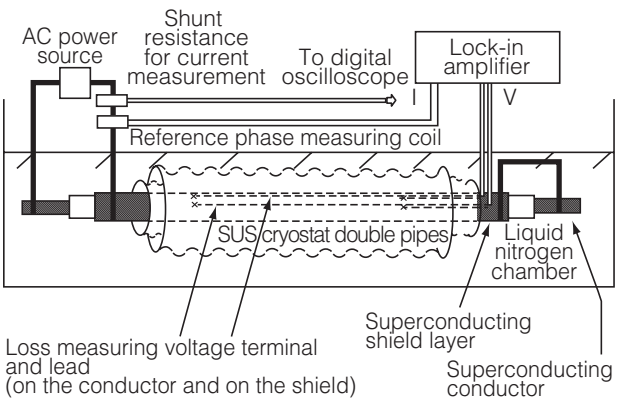

Fig. 19. Layout of measurement circuit of cryostat pipe loss.

5.3.3 Eddy current loss of multi-layered thermal insulation

The multi-layered thermal insulation wound on the inner pipe of stainless-steel cryostat double pipe shown in Fig. 4 is constructed by layering double sided tapes coated with an aluminum deposition film and insulation films. The loss of cryostat pipe was also measured with and without the multi-layered thermal insulation along with the measurement described in Section 5.3.2. No significant difference is found within the range of the measurement, showing that the eddy current loss of the multi-layered thermal insulating layer can be neglected. However, it should be noted that induced voltages would arise in the longitudinal direction if the tapes act as a spiral coil.

5.3.4 Examples of calculation under an actual usage condition

We will consider a case of the following configuration: a superconducting cable consisting of a 4-layer conductor and 2-layer shield, 22 mm for the diameter under the conductor, 40 mm for the diameter under the shield, a cryostat pipe shown in Table 2, 50 Hz for

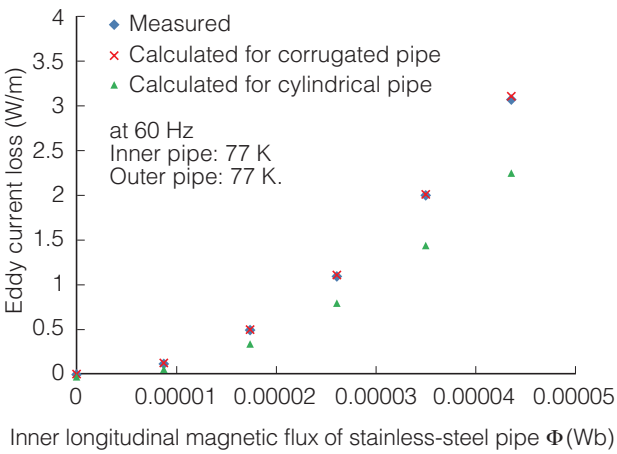

Fig. 20. Comparison of measurement and calculation for eddy current loss of SUS cryostat pipe.
(Both inner pipe and outer pipe of cryostat are immersed in liquid nitrogen.)

the frequency, and 5000 Arms for the current loading. The three cases with assumed combination of the stranding direction of the conductor and the shield and the current distribution ratio of each layer are shown in Table 3. The stranding pitch for each case is selected as appropriate. The internal axial flux interlinkage within the cryostat pipe for each of the three cases is indicated by an arrow on the horizontal axis of the graph in Fig. 21. When the target value for the loss of cable is set to 2 W/m, the eddy current loss for the case III cannot be ignored compared to the other two cases. Therefore, it is conceivable that the consideration on the eddy current loss of cryostat pipe should be included in the design of cables of single-core type when the current is increased. A comprehensive judgment is required for final design of the stranding pitch, the stranding direction, and other parameters of the conductor and the shield by taking into account manufacturability and mechanical properties of the cable.

Table 3. Assumed cases for stranding direction and current distribution ratio of each layer.

Case	Stranding direction of each layer		Current distribution ratio (%) to each layer	
	4-layer conductor	2-layer shield	4-layer conductor	2-layer shield
I	S, S, S, S	S, S	25, 25, 25, 25	−50, −50
II	The same as above	The same as above	28,42,26, 4	−65, −35
III	S, S, S, S	Z, Z	25, 25, 25, 25	−50, −50

Case I: S stranding for all the wires, uniform current distribution design
Case II: S stranding for all the wires, non-uniform current distribution
Case III: SSSS + ZZ-stranding, uniform current distribution design

S stranding: Right stranding
Z stranding: Left stranding

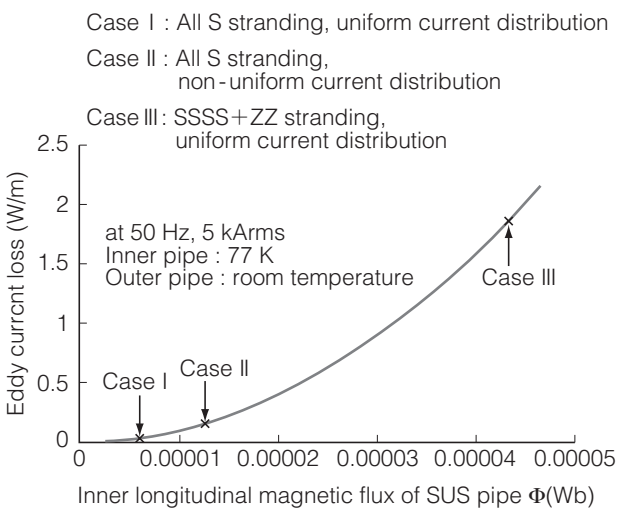

Fig. 21. Estimated results of the eddy current loss of stainless-steel cryostat pipe for actual use. (Inner pipe is filled with liquid nitrogen; outer pipe is exposed to ambient temperature)

6. Demonstration of reducing the loss of superconducting cable [3)]

Most of the measures for reducing the loss at each structural part of cable mentioned above were applied for the development of "Technology for large current and low AC loss cable" as part of an earlier NEDO project, "Technological Development of Yttrium-Based Superconducting Power Equipment."

6.1 Cable structure and target values for the loss at each structural part of cable

The structure and specifications of a 66 kV-5 kA_{rms} class single-core type superconducting cable are shown in Fig. 4 and Table 4, respectively. The target of the cable core design is set as follows: rated capacity; one phase of triple-core type of 66 kV-5 kA_{rms} class, AC loss; 2 W/m or less per phase at 5 kA_{rms}, and outer diameter of core; outer diameter of core of triple-core type which can be fit into ducts with a diameter 150 mmϕ. The cable structure is basically designed to conform to the results of the NEDO project, "Technological Development of Yttrium-Based Superconducting Power Equipment." [17)18)] The targets for the loss at each structural part are given in Table 5 along with demonstrated data, which will be described later. The loss at the stainless-steel cryostat pipe is not applicable to the triple-core type, and for certain experimental reasons, only one phase unit of the cable core was placed into a cryostat pipe for the evaluation as a single-core type cable.

6.1.1 Copper former

Actual formers are constructed by composite stranding of separate bundled wires, which are either insulated wires or resistive film wires, in order to reduce the impedance for a short-circuit current. The eddy current loss during normal operation is calculated by Eq. (13) by taking into account the stranding ratio and

Table 4. Specifications of the 66 kV / 5 kA_{rms} class single-core HTS cable.

Item	Specification
Former	Stranded copper wires (140 mm^2) 20 mmϕ
Superconducting conductor	4 layers, 59 tapes, All 4mm-width tapes (I_c = 14 kA) I_c = 240 A/4 mm-width (77 K, s.f.)
Electrical insulation	Kraft papers (6 mm-thickness)
Superconducting shield	2 layers, 53 tapes, All 4mm-width tapes (I_c = 12.7 kA) I_c = 240 A/4 mm-width (77 K, s.f.)
Copper shield	Copper tapes (100 mm^2), 2 layers, non-inductive winding
Core protection	Non-woven fabric tapes 45 mmϕ
Cryostat	Stainless-steel corrugated double pipes Vacuum thermal insulation
Jacket	Polyethylene 114 mmϕ

Table 5. Target loss value of each part of 66 kV/5 kA$_{rms}$ class single-core HTS cable and the demonstrated data.

at 77 K, 5 kA$_{rms}$

Structural part	Target value for the loss	Demonstrated data	Remarks
Former	0.1 W/m or less	0.03 W/m	Based on separate actual measurement
Superconducting conductor and shield	1.8 W/m or less	1.4 W/m	Corresponding to the loss of one phase of triple-core type cable (including the losses of the former and the copper shield)
Copper shield layer	0		Based on theoretical consideration
SUS cryostat pipe	0.1 W/m or less	0.05 W/m	Based on separate actual measurement
Overall (total)	2.0 W/m or less	1.45 W/m	

* Dielectric loss is out of scope of consideration for the current loading verification test (no voltage application) addressed in this paper.

the eddy current loss in the longitudinal direction of wires as the stranding effects of the structure. The calculated eddy current loss of the former is plotted in Fig. 22 as a function of axial magnetic flux density for different values of the diameter of former wire. The wire diameters are within the range in which the penetration of magnetic flux into the interior of copper wire caused by the skin effect can be ignored. The target for the eddy current loss is set to 0.1 W/m or less at 5 kA$_{rms}$ so as to minimize the loss. In order to satisfy the target for the loss even in case III where the magnetic field is the most severe (the conductor and the shield are stranded by SSSS + ZZ-stranding), it is necessary to select the wire diameter of 0.3 mm. In the NEDO project, enamel-coated wire, which is readily available, was used. In addition, the stranding of bundled wires of diameter 0.3 mm was a concern pertinent to manufacturing because of its small mechanical stiffness, but no particular problems arose.

6.1.2 Superconducting conductor and shield

Based on the analysis result [18] carried out in the NEDO project, "Technological Development of Yttrium-Based Superconducting Power Equipment," on the current load factor and the loss of the conductor for 5 kA$_{rms}$, the total AC loss of 1.8 W/m or less was expected by setting the load factor for the conductor and the shield to 50% and 55%, respectively. Therefore, the target values of critical current were set to 14 kA and 12.7 kA (at 77 K, s.f.) for the conductor and the shield, respectively, as shown in Fig. 23. The width of

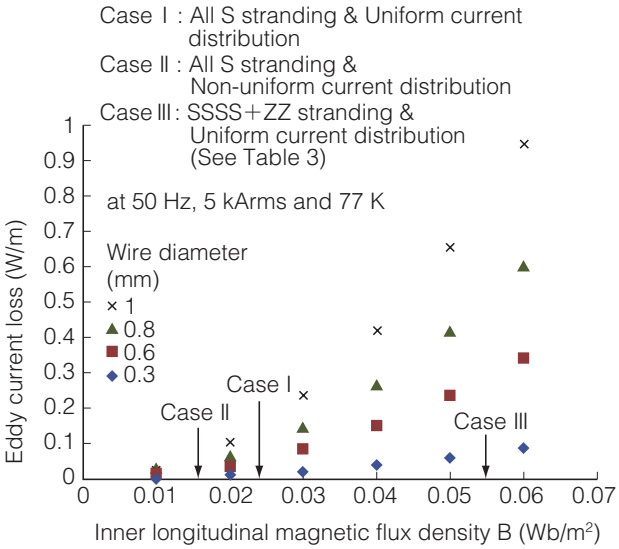

Fig. 22. Calculation result on dependence of eddy current loss of former on the diameter of each wire.

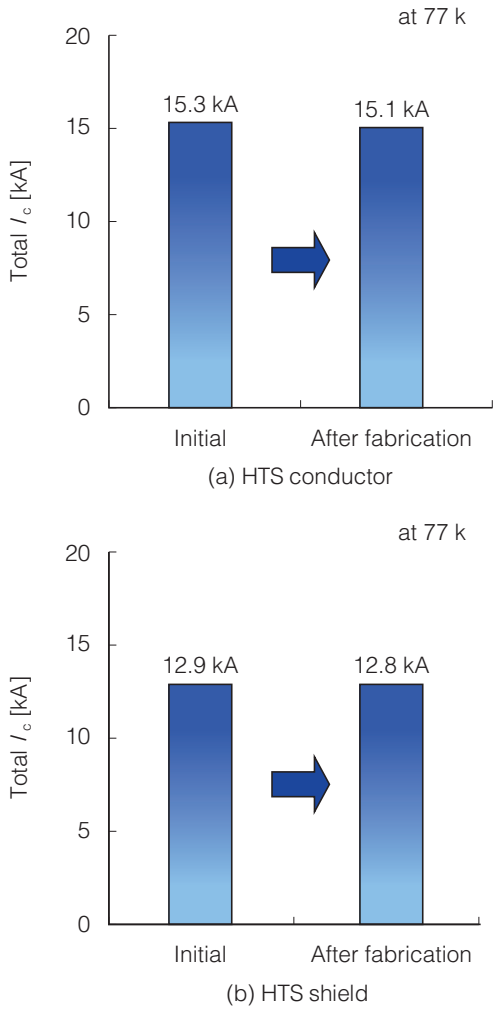

Fig. 23. Measurement results of total Ic of all Y-based tapes before and after fabrication of cable core.

all the wires for the conductor (59 wires; 4 layers) and the shield (53 wires; 2 layers) was set to 4 mm. The average critical currents per wire (I_c) were 260 A/4-

mm-w and 243 A/4-mm-w, or equivalently, 650 A/cm-w and 610 A/cm-w, respectively, which are unprecedented high critical currents. The stranding pitch design of the conductor and the shield also took into account uniform current distribution for each layer, shield layer's magnetic shielding factor for the cancellation of external magnetic fields due to the conductor current, and the eddy current loss of the former and the stainless-steel cryostat pipe.

6.1.3 Copper shield

Multiple copper strings were wound, and only one of them was insulation tape-wound to break the circumferential current loop for the purpose of preventing circumferential induced currents. Moreover, to suppress longitudinal induced voltages, non-inductive winding of an even-number (two) layer winding of SZ stranding was employed.

6.1.4 Cryostat pipe

The target value for the AC loss of cable is 2 W/m or less at 5 kA_{rms} in this verification project. Therefore, the losses for case II and case III described in Fig. 21 in Section 5.3.4 cannot be ignored, and case I, in which uniform current distribution for each layer is intended by way of S stranding for all the wires, was adopted. The loss is about 0.05 W/m.

6.2 Current loading verification test circuit for the demonstration of reducing the loss of cable

A test line included the 20 m long HTS cable, a combined terminal vessel, and a cooling system. The cooling specifications are as follows: liquid nitrogen temperature of 67K to 77K, maximum circulating flow rate of 50 L/min, and cooling capacity of 2 kW. The cable was shaped in a circular arc with a diameter of 3 m, and the two current loading ends of the cable were enclosed in a cryostat container (terminal vessel). The reason for this configuration is to suppress the impedance of the superconducting shield, so that a current of opposite phase and nearly the same magnitude as the conductor current will be induced in the superconducting shield, by shortening as much as possible the normal conducting part of short-circuit part of the

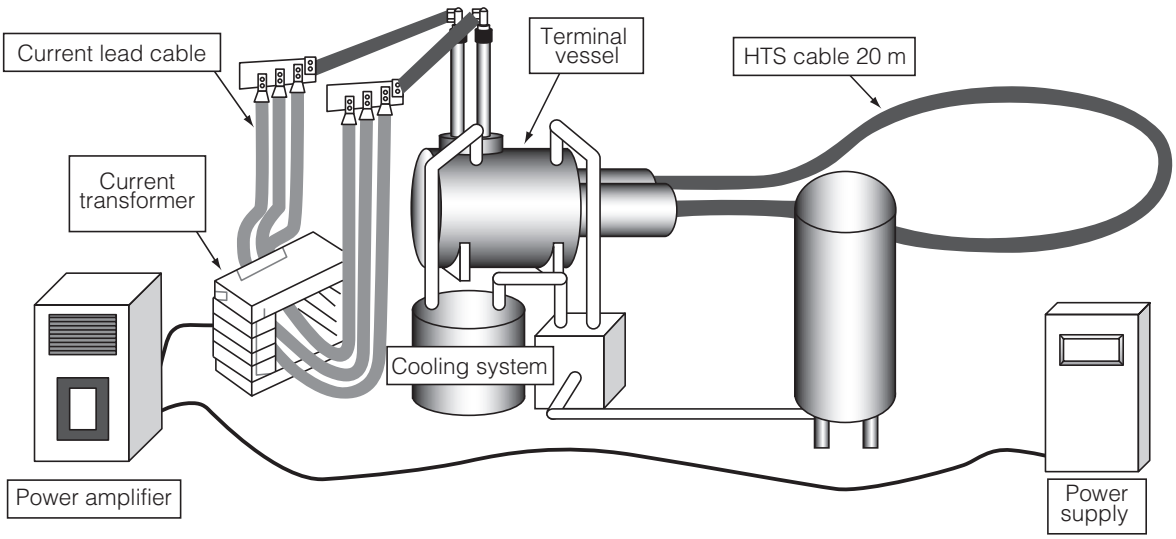

Fig. 24. Layout of current loading test line of the HTS cable.

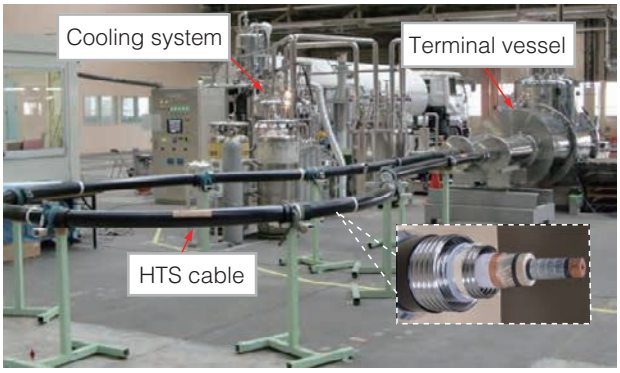

Fig. 25. The whole view of the verification system.

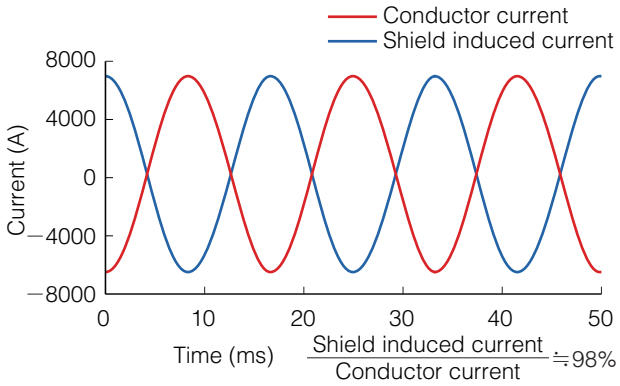

Fig. 26. Conductor current and shield induced current (at 5kA_{rms}).

shield immersed in liquid nitrogen. For the measurement of AC loss, the voltage was measured by means of AC electrical four-terminal method at the lead wire connected to the voltage terminal, which is a non-inductive lead attached to the conductor during cable manufacturing. The loss-measuring part was arranged at two places, each 8 m in length and 16 m in total, as shown in Fig. 27 (① and ②). The conductor loss, the shield loss, and the eddy current loss of the former and the stainless-steel cryostat pipe are all contained collectively in measured data.

6.3 Measurement result on reducing the losses

The current waveform of the current induced in the superconducting shield for the conductor current of 5 kA_{rms} is shown in Fig. 26. A current of about 98% of the conductor current was induced in the superconducting shield as had been planned in design. The AC loss measured at the loss-measuring voltage terminal, which is attached to the conductor, contains the loss of superconducting shield and the eddy current loss of the former and the cryostat pipe in addition to the loss of superconducting conductor. The measured loss after the extraction of the eddy current loss of cryostat pipe (0.05 W/m at 5 kA_{rms}) described in Section 5.3 is plotted in Fig. 28. Table 5 shows a comparison between the target values for the loss at each structural part of the cable at 77 K and 5 kA_{rms} and demonstrated data. The loss in which the eddy current loss of cryostat pipe is subtracted corresponds to the loss of one phase of a triple-core type cable, and sufficiently satisfies the project's target value of 2.0 W/m at 5 kA_{rms}. Furthermore, at 67 K, the loss of half the target value was achieved.

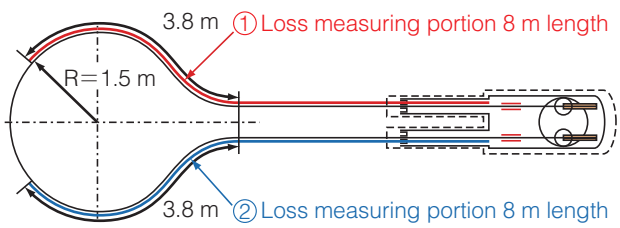

Fig. 27. Measurement portion of AC loss of the HTS cable.

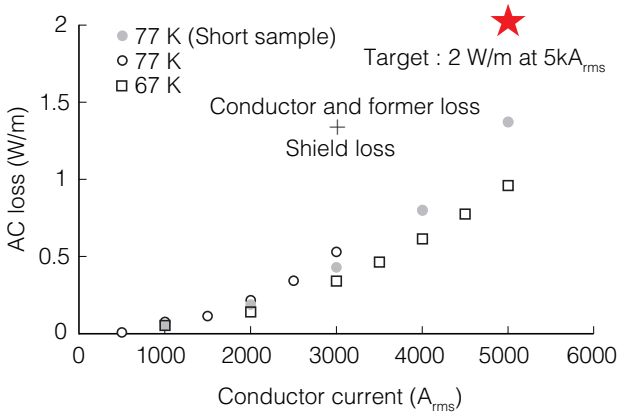

Fig. 28. Measurement result of AC loss of the HTS cable.

7. Conclusion

In general, the conductor and the shield of a superconducting cable are constructed by spirally-wound many superconducting tape wires, and an increasing number of wires are adopted when the current is increased, constituting a multi-coil structure, and in turn, giving rise to internal axial magnetic fields. Because of the magnetic field, eddy current losses arise in the copper former of an AC superconducting cable, and furthermore, eddy current loss arise in the cryostat pipe of a single-core type cable. The magnitude of the magnetic flux (loss) depends on the stranding direction, stranding pitch, and the magnitude of current, and it is conceivable that it may become non-negligible when the current is increased. Given below are the major measures described in this paper for reducing the relevant losses to reduce the overall loss of the cable:

- For reducing the loss of the superconducting conductor and shield, the loss was reduced by "reducing the current load factor" enabled by the adoption of Fujikura's original yttrium-based wire (IBAD-PLD wire) with high critical current.
- For reducing the loss of the copper former (copper stranded wire conductor), our theoretical analysis demonstrated that making the copper former of thin wires with cupric oxide (CuO) film, which has been successfully applied for currently-used cables and experimental cryogenic cables [11) 12)], is effective for reducing the eddy current loss. The film has an advantage that connection work can be simplified as compared to the case of enamel-coated thin wire.
- For the reducing the loss of stainless-steel cryostat pipe, the necessity of taking into account the eddy current loss due to internal axial magnetic flux was demonstrated analytically and experimentally. It was demonstrated that the "reducing the internal axial magnetic flux by a proper design of stranding of conductor and shield wires" is effective for the reducing the loss.

Most of these measures for reducing the losses have been reflected into the design of the 66 kV-5 kA_{rms} class cable prepared for the verification test under the NEDO project (FY2012), and the overall loss of a cable that sufficiently satisfies the target value of 2.0 W/m at 5 kA_{rms} has been achieved. In the future, it is anticipated that these measures for reducing the losses described in this paper will become increasingly important when the current is further increased.

In addition, an elliptic integral of the first kind, a complete elliptic integral of the first kind, and confor-

mal mapping were used for the analysis of the loss of copper former in this paper. A complete elliptic integral of the second kind was used for the analysis of the loss of cryostat pipe. Numerical calculation of these integrals can be readily performed at a high precision computation website on the Internet, and other computations can be completed by hand calculation.

Acknowledgments

This study lasted from August 2010 to December 2013, and part of the study was performed in FY2012 as part of a commissioned project, "Technological Development of Yttrium-Based Superconducting Power Equipment," from the New Energy and Industrial Technology Development Organization (NEDO).

We are deeply grateful to Dr. Hiroshi Suzuki (formerly at Central Research Institute of Electric Power Industry), Dr. Shotaro Yoshida, and Dr. Nobuo Shiseki (formerly at Fujikura Ltd.), who have given us various pieces of advice in performing this study. We would like to express our gratitude to Mr. Masao Saito, Mr. Tadashi Sakamoto (formerly at Fujikura Components Ltd.), Mr. Takayuki Hirasawa, Mr. Shoji Iwashita, Mr. Yutaka Hasegawa, and Mr. Shoichi Otsuka (formerly at Fujikura Ltd.), who have given us a lot of help in conducting experiments, and to Mr. Takashi Saito (formerly at Fujikura Ltd.) who has consistently guided this research and development.

References

1) Y.Iijima,et al. : "In-plane Aligned YBa2Cu3O7-x Thin Films Deposited on Polycrystalline Metallic Substrates" Applied Physics Letters, Vol.60, No.6, pp. 769-771,1992
2) M.Daibo, et al.: "World's Largest 5 T Yttrium-based High Temperature Superconducting Magnet with a 20-cm-diameter Room Temperature Bore," Fujikura Technical Review, No. 43, pp. 25-30, 2014
3) M.Yoshida, et al.: "The World's Largest 5 kA_{rms} Extremely-Low-Loss High-Tc Yttrium-based Superconducting Power Cable," Fujikura Technical Review, No. 44, pp. 41-46, 2015
4) T.Hamajima, et al.: "Analysis of Current Distribution in a Large Superconductor," TEION KOGAKU, Vol. 35, No. 4 (2000), pp. 176-183
5) NEDO Project Ledger (disclosed), FY2009 intermediate evaluation subcommittee, "High Temperature Superconducting Cable Verification Project," pp. III-27-31, November 2009
6) N. Amemiya: "AC Losses in High T_c Superconductors - AC Loss Characteristics of Tapes and Power Transmission Cables - ," TEION KOGAKU, Vol. 45, No. 8 (2010), pp. 376-386
7) N. Amemiya, et al.: "AC loss Reduction of Superconducting Power Transmission Cables Composed of Coated Conductors," IEEE Trans.Appl.Supercond. 17 (2007) 1712-1717
8) W.T. Norris : "Calculation of Hysterisis Losses in Hard Superconductors Carrying AC: Isolated Conductors and Edges of Thin Sheets," J.Phys. D: Appl. Phys. 3(1970)489-507
9) G. Vellego and P. Metra: "An Analysis of the Transport Losses Measured on HTSC Single-phase Conductor Prototypes," Supercond. Sci. Technol. 8(1995)476-483
10) K.Watanabe: "A Study on Eddy Current Loss Calculation of Conductor Former for HTS Power Cable - An Application of Elliptic Function - ," Electromagnetic Theory Symposium, EMT-11-141, 2011
11) S. Akita, et al.: "Development of external cooling cryoresistive cable systems (Part 1)
- Performance of the cooling system and the dielectric losses - ," CRIEPI Research Report, T86006, p. 13, December 1986
12) K.Watanabe, et al.: "Conductor made of insulated wire with cupric oxide film," IEEJ National Convention, No. 1148, 1979
13) K.Watanabe, et al.: "Magnetic shielding for AC superconducting cables and eddy current loss of cryostat pipe - An application of elliptic function - ," Electromagnetic Theory Symposium, EMT-13-123, 2013
14) M. Daibo, et al : "Development of a 66 kV-5kArms Cass HTS Power Cable using REBCO Tapes with Hgh Critical Current" IEEE. Trans, on Applied Superconductivity, Vol.25, No.3, 5402105, June 2015
15) K.Watanabe, et al.: "Eddy Current Loss of Cryostat Pipe of HTS Power Cable," 2013 Autumn Meeting of Cryogenics and Superconductivity Society of Japan, No. 1B, p. 07, 2013
16) K.Watanabe, et al.: "Calculation formula of eddy current loss of cryostat pipe for single core type HTS power cable - An example of utilization of elliptic function - ," IEEJ National Convention, No. 7-143, 2016
17) M. Ohya, et al.: "Development of 66 kV/5 kA Class "3-in-One" HTS Cable with RE123 Wires", Abstract of CSJ Conference ,Vol.84(2011), p.189.
18) NEDO Project Ledger (disclosed), "Technological Development of Yttrium-Based Superconducting Power Equipment," pp. III-2.2.18-19, August 2010

< Appendix >

Table of shape factor, K, in Eq. (37) in the text

The shape factor, *K*, which depends on the pitch, *p*, and the corrugation height, *h*, of a corrugated pipe, is determined as a function of a variable, h/p. The relationship is plotted in Appended Fig. 1, and the table of shape factor is shown in Appended Table 1. The values of *K* in this table represent the ratio of the length of straight pipe to the actual length of corrugated pipe.

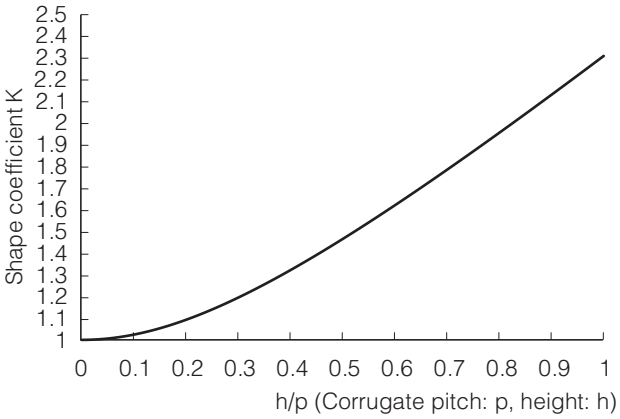

Appended Fig. 1. Graph of the shape coefficient K of eddy loss formula.

Appended Table1. Numeric table of the shape coefficient K of eddy current loss formula(37)(38).
(Dimensions of cryostat corrugated pipes: corrugation height *h*, pitch *p*, average diameter 2 r_{mean})

Condition : $h \ll 2\ r_{mean}$

h/p	K	h/p	K	h/p	K	h/p	K	h/p	K
0	1	0.2	1.0924	0.4	1.3207	0.6	1.6186	0.8	1.9519
0.01	1.0002	0.21	1.1012	0.41	1.3343	0.61	1.6346	0.81	1.9692
0.02	1.0010	0.22	1.1104	0.42	1.3481	0.62	1.6507	0.82	1.9865
0.03	1.0022	0.23	1.1199	0.43	1.3621	0.63	1.6669	0.83	2.0038
0.04	1.0039	0.24	1.1297	0.44	1.3762	0.64	1.6831	0.84	2.0212
0.05	1.0061	0.25	1.1398	0.45	1.3904	0.65	1.6994	0.85	2.0387
0.06	1.0088	0.26	1.1502	0.46	1.4048	0.66	1.7158	0.86	2.0562
0.07	1.0120	0.27	1.1609	0.47	1.4194	0.67	1.7323	0.87	2.0737
0.08	1.0156	0.28	1.1718	0.48	1.4340	0.68	1.7488	0.88	2.0913
0.09	1.0197	0.29	1.1830	0.49	1.4488	0.69	1.7654	0.89	2.1089
0.1	1.0242	0.3	1.1945	0.5	1.4637	0.7	1.7821	0.9	2.1265
0.11	1.0292	0.31	1.2061	0.51	1.4787	0.71	1.7988	0.91	2.1442
0.12	1.0346	0.32	1.2180	0.52	1.4939	0.72	1.8156	0.92	2.1619
0.13	1.0405	0.33	1.2302	0.53	1.5091	0.73	1.8324	0.93	2.1797
0.14	1.0467	0.34	1.2425	0.54	1.5244	0.74	1.8493	0.94	2.1975
0.15	1.0534	0.35	1.2551	0.55	1.5399	0.75	1.8663	0.95	2.2153
0.16	1.0605	0.36	1.2678	0.56	1.5555	0.76	1.8833	0.96	2.2332
0.17	1.0679	0.37	1.2807	0.57	1.5711	0.77	1.9004	0.97	2.2510
0.18	1.0757	0.38	1.2939	0.58	1.5868	0.78	1.9175	0.98	2.2690
0.19	1.0839	0.39	1.3072	0.59	1.6027	0.79	1.9347	0.99	2.2869
								1	2.3049